Ionics (2024) 30:2839–2850
https://doi.org/10.1007/s11581-024-05464-x

RESEARCH

# Study on velocity fields of $H_2$ during water electrolysis with KOH electrolyte comprising ionic liquid

**Clauber André Ferasso[1] · Jeferson Diehl de Oliveira[2] · Lirio Schaeffer[1]**

Received: 1 December 2023 / Revised: 16 February 2024 / Accepted: 2 March 2024 / Published online: 8 March 2024


## Abstract

This study presents an analysis of the electrolysis process using nickel–iron electrodes with a 30% KOH electrolyte and a 30% KOH electrolyte with an additional 2.5 g of ionic liquid (BMI.BF4). The electrodes were placed 20 mm apart, and the current density at 55, 110, and 165 A/m$^2$. The process involved capturing and processing images of hydrogen generation to observe the influence of the ionic liquid on ionic conductivity. Results, depicted through images of vertical velocity, vorticity, and velocity field, indicate potential gains in hydrogen generation with larger volumes of bubbles and improved vertical displacement speeds of bubbles when adding ionic liquid to the electrolyte.

**Keywords** Electrolysis · Ionic liquid · Optical flow · Hydrogen production

## Introduction

The past decade has witnessed an intense search for new energy sources, preferably renewable or green energy. In order to alleviate the current electrical energy generation system. While batteries and capacitors are suitable for short-term electricity storage, long-term storage can be achieved through the use of hydrogen. In these cases, electricity produced from renewable sources would be used to power the electrolyzers, thus being converted into hydrogen through water electrolysis, being one of the best storage systems in terms of environmental sustainability. The hydrogen produced can be stored using pressurized tanks, for example, and converted back into electricity when necessary. In this way, the use of hydrogen as an energy vector allows the storage of excess energy during generation peaks from renewable sources and the production of energy during energy deficit phases [1, 2]. The concept of energy generation through water electrolysis leading to hydrogen production has gained prominence over the years. In recent years, there have been significant advancements in electrolysis technology, especially in the development of more efficient and cost-effective electrolyzers, along with the increasing availability of renewable energy sources such as solar and wind power, which can be used to power the electrolysis process. This may make electrolysis more competitive in terms of cost and environmental sustainability. Hydrogen production through water electrolysis is a crucial technique undergoing continuous improvement through research, resulting in cost-effectiveness. This improvement involves selecting suitable electrodes and electrolytes to enhance efficiency in the hydrogen generation process [3, 4]. The costs associated with hydrogen production can be mitigated by scaling up the generation of low-cost renewable electricity, amplifying the energy output of renewable sources, and enhancing electrolyzer efficiency through the utilization of high-performance materials [5]. While hydrogen is not naturally found in its free form, it is combined with other chemical elements in various molecules, necessitating chemical processing for extraction [6]. Traditionally, hydrogen is produced from fossil resources, primarily methane (natural gas), due to cost efficiency. However, concerns about depleting fossil fuel reserves and increasing gas prices have shifted focus to alternative hydrogen production methods [6, 7]. Among various electrolyzer technologies, alkaline electrolyzers have proven to be highly successful from a commercial

✉ Clauber André Ferasso
clauber.andre@gmail.com

[1] PPGE3M - Postgraduate in Mining, Metallurgical and Materials Engineering, Federal University of Rio Grande do Sul – UFRGS, Porto Alegre, Rio Grande Do Sul, Brazil

[2] SISEA - Renewable and Alternative Energy Systems Laboratory, Polytechnic School of the University of São Paulo, São Paulo, Brazil

perspective due to their simplicity and cost-effectiveness. Despite already being in commercial use, research on alkaline electrolyzers remains dynamic, focusing on optimizing their operation and enhancing overall efficiency [8]. The electrolysis of water is widely used to produce hydrogen with a very high degree of purity. It is a relatively simple process, which depends on drying and eliminating impurities from the gas [9, 10]. Hydrogen production through water electrolysis requires improvements in energy efficiency, safety, durability, operability, portability, and the reduction of installation and operation costs [11]. This process involves the application of a direct electric current, leading to the dissociation of water molecules through redox reactions, resulting in the generation of hydrogen and oxygen gases [12]. The electrolysis of water involves the separation of its molecules into hydrogen and oxygen gases through the passage of a direct electric current. The current flows between two separate electrodes immersed in an electrolyte, which increases the ionic conductivity of the medium. The electrodes, and electrolyte are elements that configure the electrolytic cell [13]. In fact, during water electrolysis, the proportion of hydrogen ($H_2$) and oxygen ($O_2$) produced is 2:1. This means that for every molecule of oxygen produced, two molecules of hydrogen are produced. This ratio is based on the chemical equation of the water electrolysis reaction (i.e., $2H_2O \rightarrow 2H_2 + O_2$). The energy density of hydrogen is approximately 120 MJ/kg, while that of coal, for example, ranges between 24 and 35 MJ/kg. In terms of sustainability and environmental impact, hydrogen production from renewable sources releases only oxygen ($O_2$) as a by-product, with no carbon emissions. Hydrogen stands out as a promising carrier of clean and sustainable energy due to its high energy density, surpassing that of typical solid fuels [14]. The significant challenge in hydrogen production from water electrolysis lies in finding materials for electrolytes and electrodes that offer high performance at a low cost or enhance existing ones. Ni alloys with different metals have been studied. It has been demonstrated that NiCo alloys have better electrocatalytic performance compared to pure Ni and Co electrocatalysts. Similar conclusions were obtained in the case of NiFe for the occurrence of hydrogen evolution [2].

Ionic Liquids (ILs) composed of ionic species, cations, and anions, are considered green solvents with low or no vapor pressure and high chemical stability. Their physical–chemical properties make them suitable for various chemical reactions, and their recyclability further enhances their utility. ILs have demonstrated high performance in clean energy generation reactions, particularly as electrolytes in water electrolysis for hydrogen production and in fuel cells [15]. To contribute to $H_2$ production, ILs are particularly relevant. Operating as molten salts below 100 °C, ILs comprise ionic species, cations, and anions. Their green solvent properties, low or no vapor pressure, and high chemical stability make them versatile for different chemical reactions, primarily due to their recyclability [16, 17].

ILs perform well in clean energy generation reactions, especially when compounded with potassium hydroxide (KOH), acting as electrolytes in the electrolysis of water to produce hydrogen, in batteries and fuel cells [17–20].

The utilization of hydrogen production technology through water electrolysis considers its application as a vector, but, more importantly, it generates minimal impact on the environment and can be obtained through non-complex processes. The choice to use Ni–Fe electrodes is linked to the necessity of employing vast and nature-friendly components that have efficient effects and meet the desired demand. Currently, the majority of available hydrogen originates from these reactions catalytically [21]. Alkaline electrolyzers are well-developed for production from renewable sources at significant rates; however, in the context of the hydrogen economy, the production capacity of electrolysis units needs to surpass the current capacity. These factors drive research and development for hydrogen production through water electrolysis [10–22]. To evaluate different electrolysis systems, it is necessary to relate a series of practical parameters to the performance of various electrolyzers. Important parameters include the $H_2$ generator settings and operating conditions. Therefore, studies dealing with the hydrodynamics of water electrolysis at different current densities in various generator scenarios can modify the homogeneity of gases [23, 24]. The gas bubbles that grow in contact with electrodes have multiple impacts on the electrochemical process; they are intermediate reactions. Bubbles within a layer adhered to the electrode block a fraction of the cross-sectional area available for current transport. The actual current density is greater than the nominal. Therefore, the energy demand of the cell is affected. The electrode potential changes due to the electrochemical reaction, as well as its ohmic resistance [24]. Bubbles growing and detaching from the electrode induce micro convection in the boundary layer, intensifying mass transfer. Furthermore, bubble coverage controls the area of the gas–liquid interface and affects liquid dissolution, contributing to bubble growth [25]. The use of ionic liquid IL in the electrolyte offers the ability to increase current density in the circulation process between electrodes. However, they are often limited by low solubility levels and low conductivity [10]. Some ILs have characteristics similar to non-aqueous organic solvents, such as low volatility, high thermal stability, acceptable conductivity, as well as greater solubility of active species [18, 19]. The main properties of IL are related to high ionic conductivity, non-flammability, potential without oxidation or reduction, low thermal variation, among others. Chemical stability, associated with negligible vapor pressure and electrochemical characteristics, provide ILs with expressive electrical potentials, with a low capacity to generate gases

[26]. In particular, the IL 1-butyl-3-methylimidazolium tetrafluoroborate—BMI.$BF_4$ (shown in Fig. 1) is an ionic liquid belonging to the imidazole class. It is commonly used as an ionic solvent in various applications and some of its important characteristics include thermal and chemistry stability, making it suitable for various reactions and processes, including chemical synthesis, electrochemical catalysis, and electrochemical applications. It is also known that BMI.$BF_4$ has been shown high conductivity [27, 28]. This makes it an interesting component to be used in increasing the efficiency of electrolysis, due to the increased current density at reduced voltage ranges at room temperature, for example [29]. The choice of LI BMF.$BF_4$ was due to publications on this compound in energy areas such as capacitors, fuel cells, and electrolysis [20, 30–32]. It is understood to have suitable specific characteristics such as viscosity, conductivity, and solubility.

Various techniques have been employed for the analysis of both hydrogen production and bubble dynamics during water electrolysis, including optical methods. Indeed, there are different methods of capturing images and measurements through the use of optical techniques for image acquisition, as the processing of images is necessary to complement the analysis. Some methods can be highlighted, such as Particle Image Velocimetry (PIV). The PIV system is based on four components and software: pulse laser, digital camera, synchronizer, high-speed image acquisition board, image analysis, and processing software. Laser Doppler Velocimetry (LDV), in addition to the equipment described, requires specific dyes to locate the released gases, and Digital Particle Image Velocimetry (DPIV), which uses laser light and a digital camera to record the successive positions of particles [23–25, 20, 26–34]. This study utilizes the optical flow method to examine the dynamics of hydrogen generation through water electrolysis, exploring the impact of current density and of the ionic liquid BMI.$BF_4$.

The analyses specify absolute values referring to each stage of the research through the graphs generated, thus allowing the quantification of gains at each current density applied to the electrolytes formed by 30% KOH and 30% KOH added with IL. The results, as illustrated by the presented scenarios, indicate gains of up to 50% in vertical speed, representing a higher number of hydrogen bubbles,

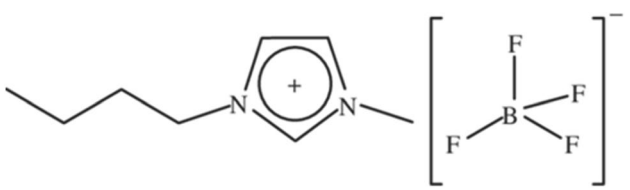


**Fig. 1** Molecular structure of 1-butyl-3-methylimidazolium tetrafluoroborate—BMI.$BF_4$

the use of IL can increase ionic conductivity during electrolysis, reducing the need for electrical energy consumption in hydrogen generation. Additionally, they demonstrate, in a positive and innovative manner, the utilization of the optical flow method to generate results.

## Experimental section

To conduct the hydrogen generation experiment through water electrolysis, a polylactic acid (PLA) support was developed using a 3D printer to secure the Ni–Fe electrodes. For this stage, the casing was removed, and the electrolyte was poured into the glass container described earlier. The electrical current to power the electrodes was supplied by a DC source. To record and identify hydrogen generation, images were taken using a Canon camera, model EOS 5D Mark III, with a 100 mm macro lens, stabilized on a support. The images were processed to be represented through computer graphics, as shown in Fig. 2. This configuration consists of a test section that includes a cubic container (electrolyzer) with a capacity of 600 ml, a DC power supply model Minipa MPL-3305. The working vertical electrodes are made of Ni and Fe. The choice of this material is due to its stability in an alkaline environment.

Both electrodes are 75 mm wide and 90 mm long, arranged vertically with a distance of 20 mm between them. The experiment was carried out at room temperature, approximately 23 °C, with an aqueous solution of KOH at 30% in relation to deionized water, inside a glass container (electrolyzer) with 100 mm × 12 mm × 90 mm. The tests were repeated with the addition of 2.5 g of IL BMI.$BF_4$ in the electrolyte, using a mix. The current density of 55, 110, and 165 A/$m^2$, with voltage ranging between 3 and 8 V, depending on the concentration of IL. The weight was determined as a reference to the author [28–30, 20, 31–34] in which to use the IL in capacitors, with a molar fraction between 0.20 and 0.40 and presented conductivity ($\sigma$) greater than 15 mS/cm at 30° C. The solubility constant of IL is $K = 3.0 \times 10^{-3}$ mol/L [35] and viscosity between 50 e 60 mPa·s [36]. During the tests, different applied current densities were formed, and as a result, all images were captured with a resolution of 3840 × 2560 pixels and a 100 mm lens. And for the analysis of the resultant velocity field, pairs of sequentially captured images were used in the optical flow method.

### Optical flow method

Optical flow method provides several advantages in many studies related to motion investigation, and notable progresses

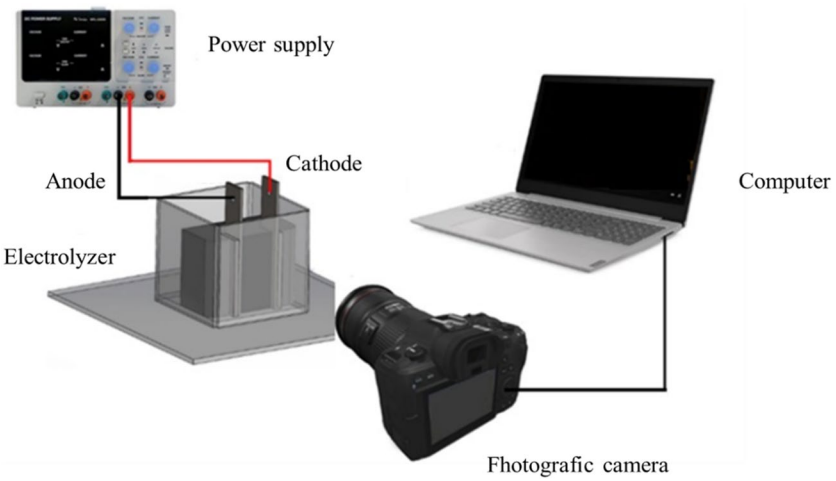


**Fig. 2** Experimental setup

have been achieved during last years [37–41]. These techniques demonstrate exceptional performance in tracking and motion analysis, allowing for the identification and segmentation of objects through consistent motion patterns. Remarkably, optical flow has the capability to function in real-time, making it well-suited for tasks that demand swift video analysis, such as bubble generation, for example. Its versatility and practicality render optical flow an indispensable tool in the realm of computer vision, facilitating the analysis and comprehension of dynamic visual information. In this study, the optical flow utilized is derived from the methodology introduced by [42]. This approach addresses the optical flow equation for various flow visualizations, articulated in terms of image coordinates:

$$\frac{\partial g}{\partial t} + \nabla \cdot (gu) - f(x, y, g) = 0 \tag{1}$$

Here, $g$ signifies the normalized image intensity, which is proportionate to the radiance received by the camera. The velocity in the image plane, indicated as $\boldsymbol{u}=(u_x, u_y)$, is termed the optical flow. The operator $\nabla \equiv \frac{\partial}{\partial x_i}$ represents the spatial gradient, while $f(x, y, g)$ corresponds to a boundary and diffusion term. Optical flow does not demonstrate divergence-free characteristics, i.e., $\nabla \bullet u \neq 0$. However, in conditions where $f(x, y, g) = 0$ and $g\nabla \bullet u = 0$, Eq. (ddd) simplifies to the Horn-Schunck brightness constraint equation $\frac{\partial g}{\partial t+u\bullet\nabla g=0}$, as described in [43]. The optical flow data analysis was conducted using MATLAB™, utilizing the open-source code offered by [44], which was developed to calculate the instantaneous velocity field from consecutive pairs of images.

## Results and discussion

The use of NiFe electrodes are considered low-cost electrocatalysts to promote good results in the occurrence of hydrogen generation [5] Other interesting results were obtained by [45, 46]. using different types of NiFe-based composite electrocatalysts. In the same way that the authors [30, 20, 31] obtained attractive results with the use of LI BMI.$BF_4$ in electrolyzers for hydrogen generation.

Initially, 2-s videos of bubble generation were recorded from each current density applied to the electrodes. These images were divided to form a set of images for each video. In this way, 02 images were selected, the "pair" for processing and generating graphics. The computational model used to compile the information was Matlab, which runs a script for optical flow analysis entitled "Flow_Diagnostics_Run." A pair of sequential images are loaded into the program. These images are then pre-processed, generating the computational optical flow, and the results will be plotted and represented by vertical velocity graphs, which demonstrate the velocity of the bubbles at 4 different heights: 1 mm, 16 mm, 32 mm, and 48 mm. They are from top to bottom, the vorticity that demonstrates the disturbance in the fluid generated by the movement of the bubbles and the velocity field graph that shows through vectors the density, volume, and trajectory of the bubbles to the top of the container. Figure 3 shows the "pairs" of images uploaded to the system for processing, showing millimetric differences in the height of the balls. Figure 3 (a) and (b) represent application of current density of 55 A/$m^2$, Fig. 3 (c) and (d) applied current density of 110 A/$m^2$, and (e) (f), with 165 A/$m^2$ of current applied. In this configuration, the electrolyte used was 30% KOH.

Figure 4 shows the model and shows the "pairs"' of images uploaded to the system for processing, showing millimetric differences in the height of the balls. Figure 4 (a) and (b) represent application of current density of 55 A/$m^2$, Fig. 4 (c) and (d) current density of 110 A/$m^2$, and (e) (f), with 165 A/$m^2$ of current applied. In this configuration, the electrolyte used was 30% KOH + 2.5 g of IL.

The sequence of images in Fig. 5 shows the vertical velocity of the hydrogen bubbles analyzed at different depth distances from the electrode (1 mm, 16 mm, 32 mm,

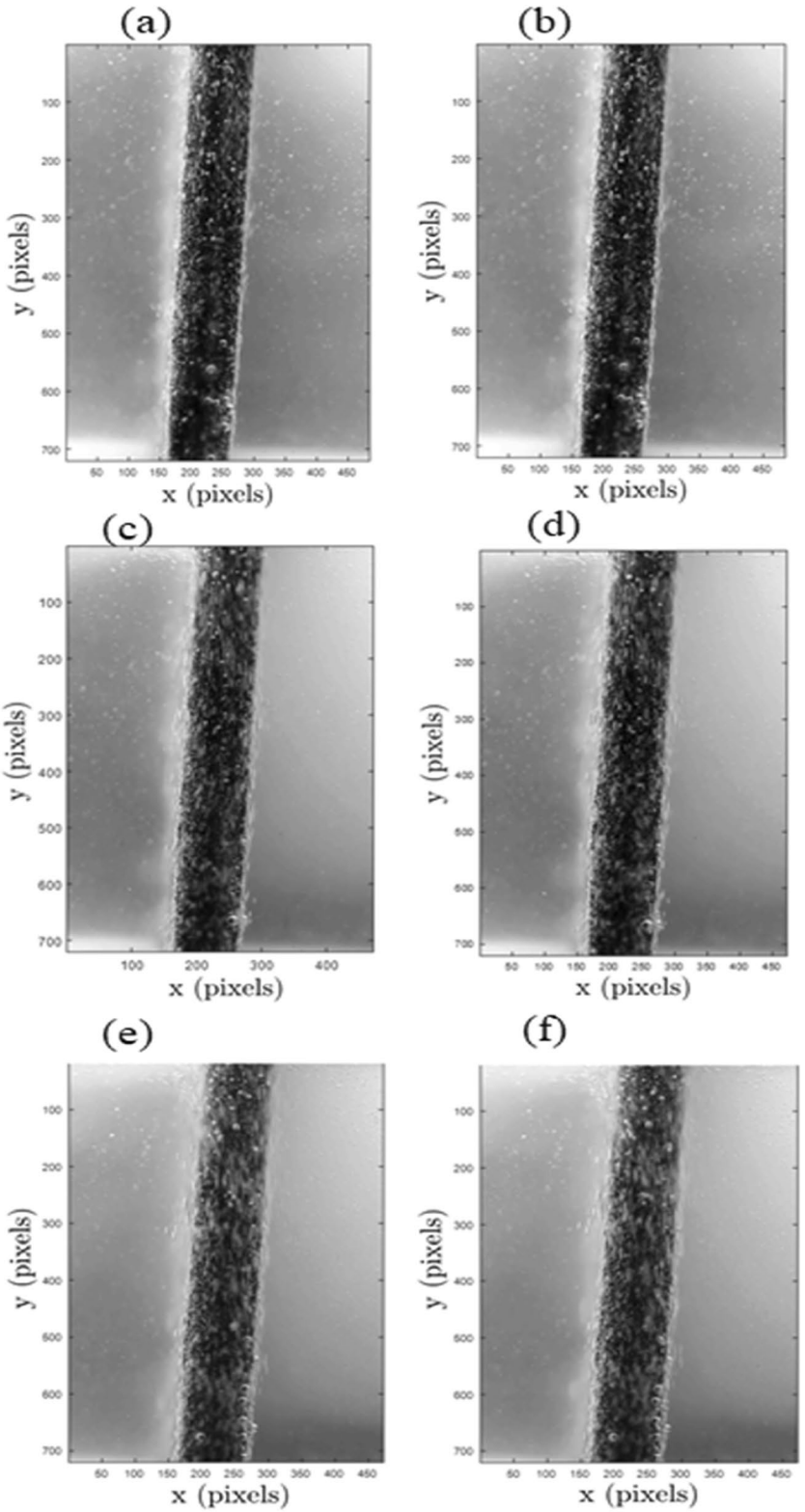


**Fig. 3** Iron anode with 30% KOH electrolyte for *J* equal to **a–b** 55 A/m$^2$, **c–d** 110 A/m$^2$, **e–f** 165 A/m$^2$

and 44 mm). The variations in the graphs represent the movement of the fluid at the ends of the electrode. The gas (bubble) released at the base rises due to buoyancy near the electrode, generating a rotational movement toward the upper part of the electrolyte volume. Figure 5 (a) and (b) show the alternation of rotational movements of hydrogen bubbles in the 30% KOH electrolyte and with the addition of IL at current density of 55A/m$^2$.

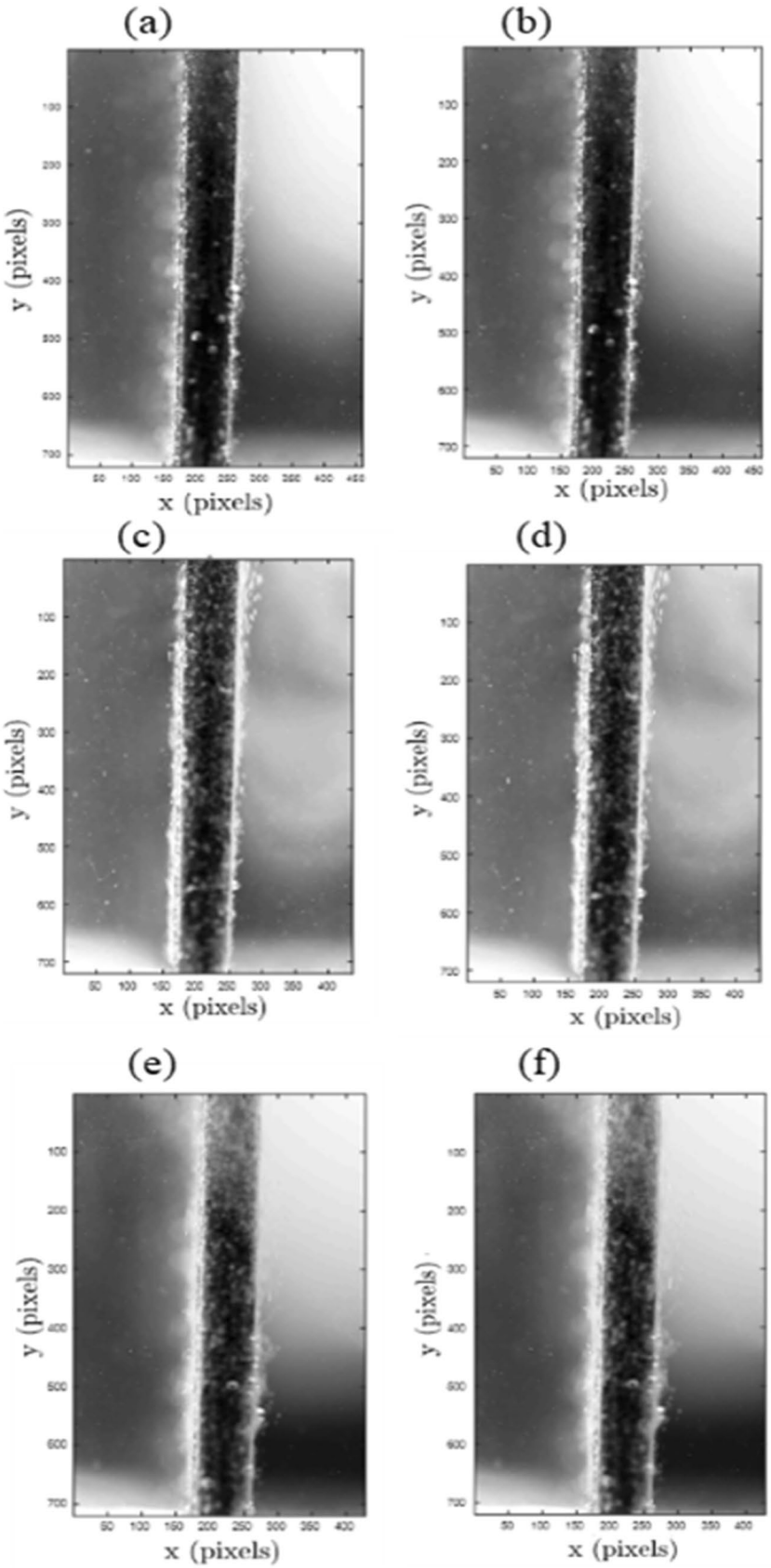


**Fig. 4** Iron anode with electrolyte KOH 30% + IL for *J* equal to **a**–**b** 55 A/m$^2$, **c**–**d** 110 A/m$^2$, **e**–**f** 165 A/m.$^2$

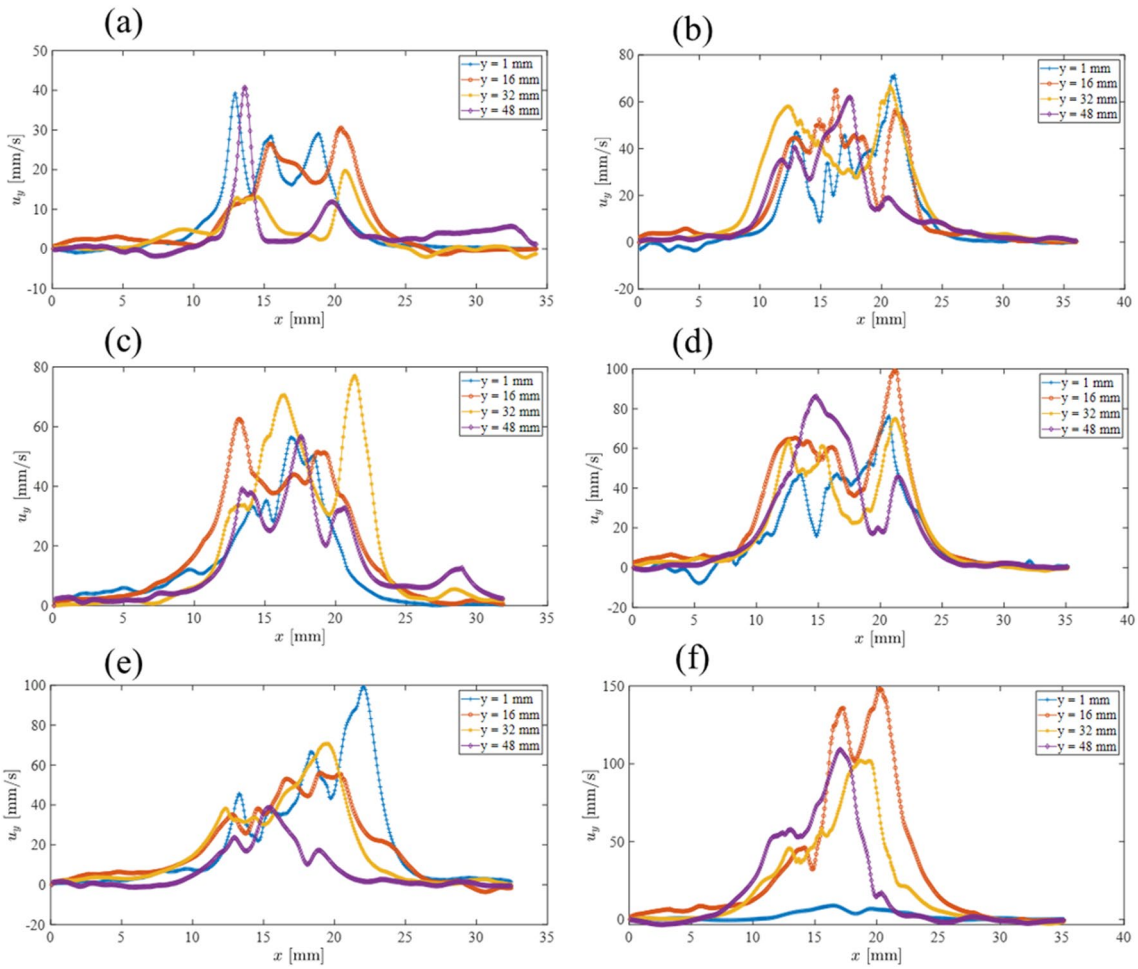


**Fig. 5** Vertical velocity in standard electrolyte (**a**–**c**–**e**) and IL-compound electrolyte (**b**–**d**–**f**), for equal current density (**a**–**b**) 55 A/m$^2$, (**c**–**d**) 110 A/m$^2$, (**e**–**f**) 165 A/m$^2$

In Fig. 5 (a), the highest speeds, around 40 mm/s, are at depths of 1 mm and 48 mm, i.e., at the base and top of the electrode. In Fig. 5 (b), with composite electrolyte, at the same depths, the speed obtained gains, changing to 60 mm/s and 70 mm/s. It is also noted that the intermediate velocities increased due to the effect of the ionic liquid, producing greater conductivity. With a current density of 110 A/m$^2$, the variation of the maximum points in Fig. 5 (c) is between 65 and 80 mm/s, belonging to intermediate depths of 16 mm and 32 mm; at depths of 1 mm and 48 mm, the speeds were close, around 60 mm/s. In Fig. 5 (d), the speeds obtained gains at all depths, the highest between 85 and 100 mm/s, respectively at 48 mm and 16 mm. Figure 5 (e–f) shows vertical speed with an applied current density of 165 A/m$^2$, indicating the alternation of rotational movements of hydrogen bubbles in the 30% KOH electrolyte and with the addition of ionic liquid. In Fig. 5 (e), the highest bubble speeds are close to the surface at a depth of 1 mm, with a speed of 100 mm/s. With composite electrolyte, Fig. 5 (f) at a depth of 16 mm, the speed reaches 150 mm/s. There is almost no displacement of bubbles near the surface. The speeds increase with the addition of ionic liquid to the electrolyte, but there is no pattern in relation to the depths, as the current increases or with a compound electrolyte; the gains in speed may vary at depths close to the surface or close to the base of the electrode.

Figure 6 displays the vorticity of the fluid, in standard electrolyte (a–b–e) and IL-compound electrolyte (b–d–f), with current density of (a–b) 55 A/m$^2$, (c–d) 110 A/m$^2$, and (e–f) 165 A/m$^2$. Following the same distribution criteria as the images from the vertical velocity analysis. The fluid's vorticity represents its movement through the rotation of bubbles at the end of the electrode and the velocity field, indicating trajectories with varying concentrations and strengths of the movement of hydrogen bubbles. It is observed that turbulent zones are present in the central part of the images, forming practically two lines of vortices. This illustrates the disturbance caused by the bubbles as they

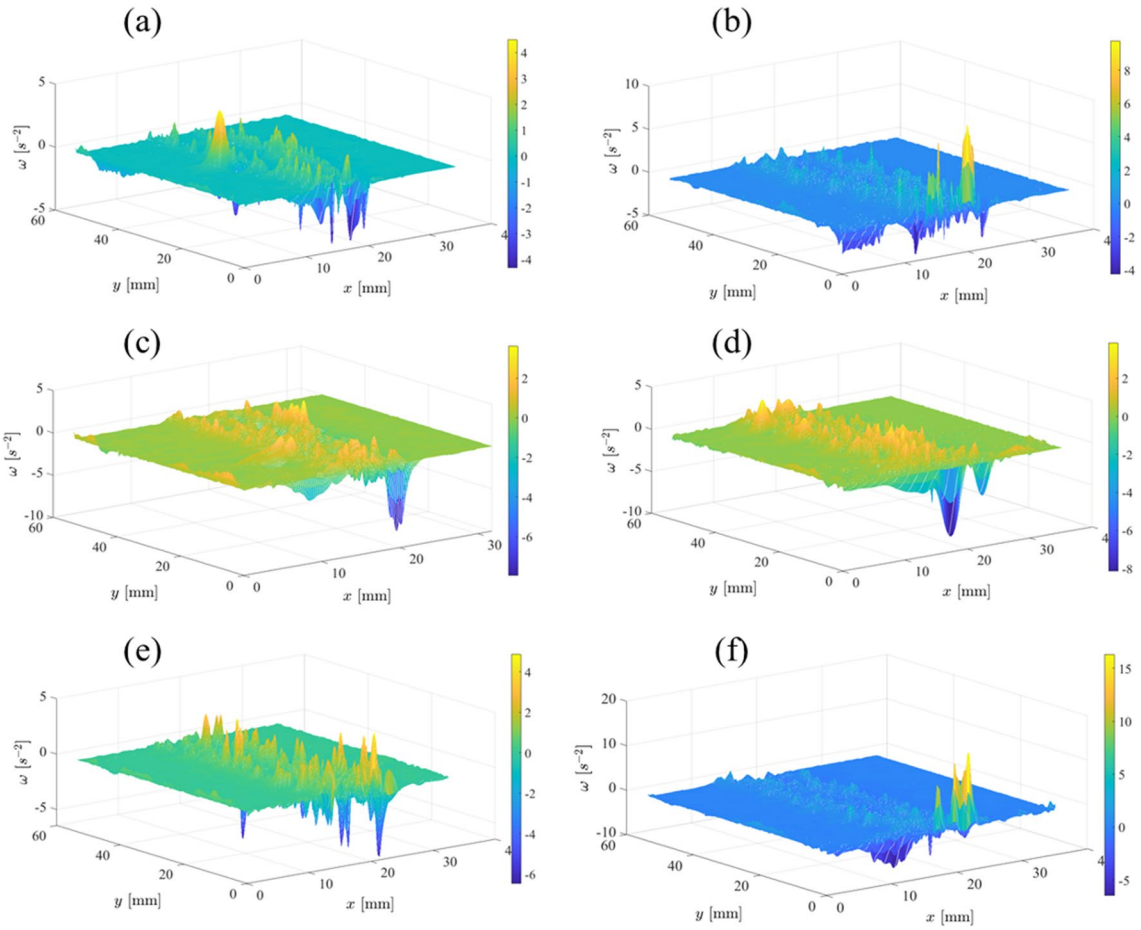


**Fig. 6** Fluid vorticity in standard electrolyte (**a**–**c**–**e**) and IL-compound electrolyte (**b**–**d**–**f**), for equal current density **a**–**b** 55 A/m$^2$, **c**–**d** 110 A/m$^2$, **e**–**f** 165 A/m$^2$

ascend to the top of the container. Turbulence occurs very close to the electrode on both sides, near the container's side, and close to the cathode. High differences in turbulence are not notable, as there is a decrease in ohmic resistance in the inner part of the electrode anode cathode, due to the reduction in distance and consequently, current circulation. Vorticity generates reflux situations in the fluid flow, which can create zones with reverse velocities, contrary to the direction of flow. The vortex occurs due to void fractions or differences in pressure in different regions.

Naturally, the fluid tries to balance the volume of the fluid, each time changing the direction. Enhancing ionic conductivity results in greater quantities of hydrogen bubbles, with higher velocities, causing changes in turbulence and disturbances in the direction of the bubble. Thus, generating reflux situations in the fluid flow, which can create zones with reverse velocities, contrary to the direction of flow. These reflux zones can also be observed in the velocity field images. The increase in the applied electrical current, similar to the vertical speed, which in this case increases, can generate more vortices and form these reflux zones, due to the change in energy in the process. Vortices help dissipate energy caused by turbulence with greater energy density.

Recirculation zones form due to differences in the electrochemical reaction rate along the electrode surface. In areas where the electric current is more intense, there is a greater generation of hydrogen gas. This released gas can create bubbles that move upward toward the electrolyte surface. As the bubbles approach the surface, they may interact with the surrounding liquid current, resulting in the formation of recirculation zones. Additionally, turbulence between the electrodes is caused by the release of hydrogen and oxygen gas during electrolysis. As gas bubbles form on the electrodes and move upward, they can disturb the flow of the electrolyte liquid. This creates regions of turbulence where the liquid circulates irregularly and chaotically. These recirculation zones and turbulence can affect the efficiency of electrolysis, as they can cause a non-uniform distribution of gases and electrolyte around the electrodes. This can lead to a lower

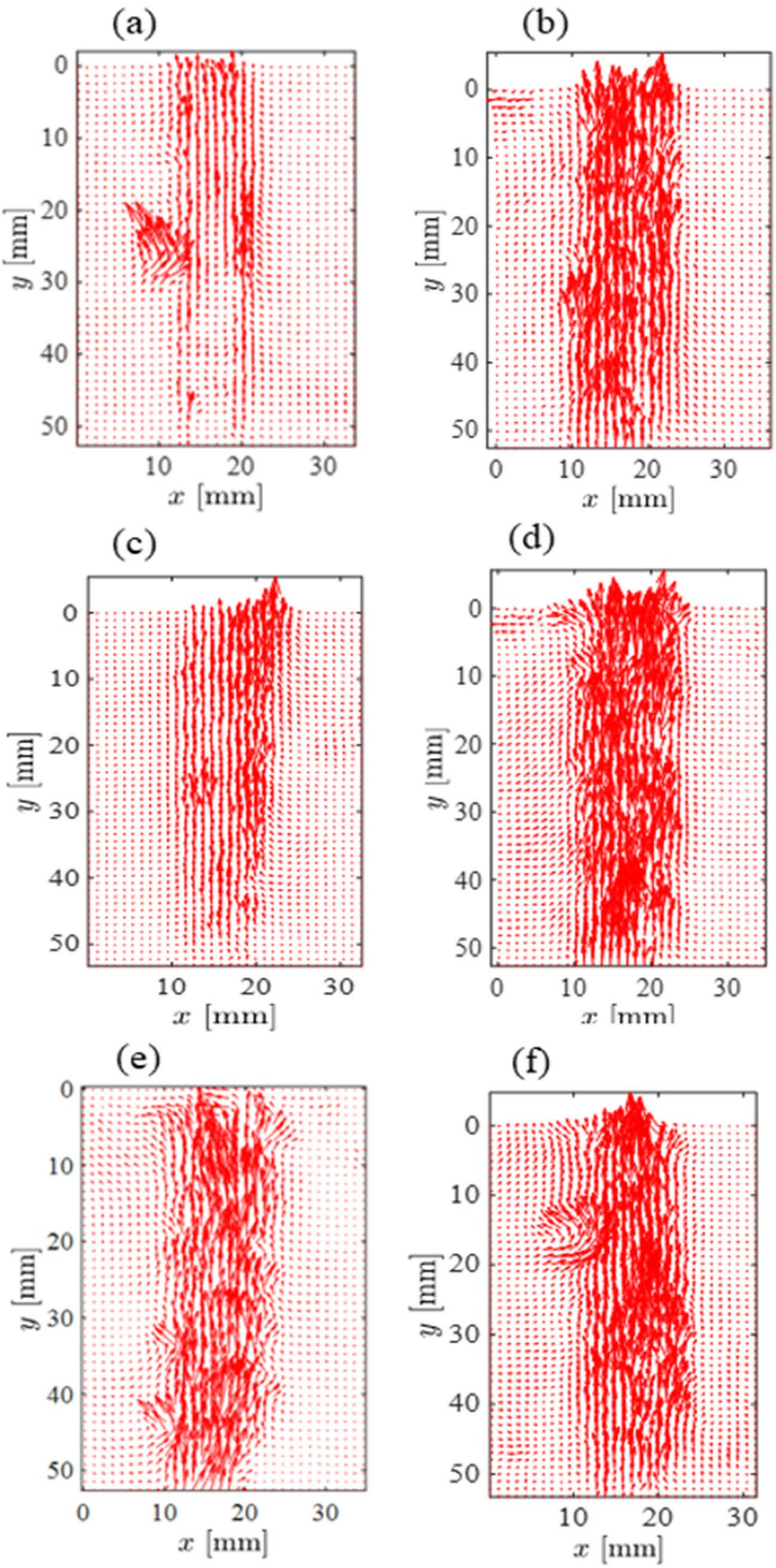


**Fig. 7** Velocity field standard electrolyte (**a**–**c**–**e**) and IL-compound electrolyte (**b**–**d**–**f**), for equal current density (**a**–**b**) 55 A/m$^2$, (**c**–**d**) 110 A/m$^2$, (**e**–**f**) 165 A/m$^2$

hydrogen production rate and higher energy loss due to system resistance. Therefore, understanding and controlling these phenomena are important for optimizing the hydrogen generation process by electrolysis. Strategies to minimize these effects include proper electrode design and optimization of operating conditions such as current density and electrolyte agitation.

The concentration of displacement of hydrogen bubbles and their direction is shown in the images in Fig. 7 through the velocity field. Although most bubbles rise to the top of the surface, some bubbles tend to migrate from the electrode to the edges. The largest vectors are distributed vertically in the images, representing greater turbulent intensity in this region, which is closer to the electrode that generates the bubbles.

The different directions of the vectors in the fields show the different trajectories of the fluid particles, highlighting the turbulent movement. Although there is also a force in the clockwise rotating flow driven by the hydrogen bubbles, it compels some bubbles to change their trajectory. This is the result of the higher current density applied and with an electrolyte composed of ionic liquid, the large number of bubbles formed on the surface of the electrode can make it difficult for hydrogen bubbles to leave or approach, as they tend to rise, creating resistance.

In Fig. 7 (a), the applied current density of 55A/m$^2$ generates bubbles with greater intensity in the center and upper part of the electrode. In the center, it is noted that there is a detachment in the direction of the bubbles, causing them to disperse from the volume of the electrodes. In Fig. 7 (b), with the addition of IL, the ionic combination of the electrolyte and ionic liquid increases the volume and number of bubbles and also the turbulence, providing an electrolyte with superior ionic mobility. Another important point is the distribution of the bubbles across the surface of the electrode and toward the top of the container. Figure 7 (c–d) shows the concentration and direction of hydrogen bubble displacement with a current density of 110 A/m$^2$, while Fig. 7 (e–f) depicts a current density of 165 A/m$^2$.

Depending on the direction of the vectors in the images, the highest concentration of bubbles tends to rise to the top of the surface. Some bubbles, due to turbulent agitation, move to the edges. It is observed that as the current density increases, the number of vectors also increases, generating greater turbulence due to the greater number of bubbles with higher vertical velocities. Improvements in these parameters are also observed in images of electrolytes composed of ionic liquid. When comparing the results of the images pair by pair, applying the same current density to ionic liquid potentiated the ionic combination of the electrolyte, reducing resistance, and thus facilitating the transport of ions through the aqueous medium.

## Conclusions

The results demonstrate the possibility of enhancing an electrolyte by adding ionic liquid, forming a compound with greater ionic stability, positively altering the results in the generation of hydrogen with a greater volume and density of bubbles, higher speed, and flow in the direction of the bubbles, and less dispersion around the center or side of the container. In the three electrical current densities applied in the experiments, there was a gain when comparing the standard and composite electrolyte with ionic liquid. The relationship between increased speed and turbulence with the addition of ionic liquid to the electrolyte is also notable. The images of the velocity fields represent this gain due to the decrease in resistance, increasing ionic circulation. The vertical speed ranged from 100 to 150 mm/s at a current density of 165 A/m$^2$. The current is influenced by the IL in the aqueous solution, generating greater ionic mobility, reducing resistance and increasing conductivity, resulting in greater displacement speed and an increase in bubbles.

**Author contribution** All authors contributed to the research. CF and JO created the research structure. LS and JO contributed knowledge and information on the subject. CF carried out the necessary tests and everyone prepared the.

**Data availability** No datasets were generated or analyzed during the current study.

## Declarations

**Ethical approval** Not applicable.

**Competing interests** The authors declare no competing interests.

## References

1. Patella B, Zanca C, Ganci F, Carbone S, Bonafede F, Aiello G, Miceli R, Pellitteri F, Mandin P, Inguanta R (2023) Pd-Co based electrodes for hydrogen production by water splitting in acidic media. Materials 16:474. https://doi.org/10.3390/ma16020474
2. Ganci F, Buccheri B, Patella B, Cannata E, Aiello G, Mandin P, Inguanta R (2021) Electrodeposited nickel-zinc alloy nanostructured electrodes for alkaline electrolyzer. Int J Hydrogen Energy 47:11302–11305. https://doi.org/10.1016/j.ijhydene.2021.09.221
3. Buccheri B, Ganci F, Patella B, Aiello G, Mandin P, Inguanta R (2021) Ni-Fe alloy nanostructured electrodes for water splitting in alkaline electrolyzer. Electrochim Acta 38:138588. https://doi.org/10.1016/j.electacta.2021.138588
4. Oliver P, Bourasseau C, Bouamama B (2017) Low-temperature electrolysis system modelling: a review. Renew Sustain Energy Rev 78:280–300. https://doi.org/10.1016/j.rser.2017.03.099
5. Carbone S, Projetto F, Bonafede F, Oliveri LR, Patella B, Gandi F, Aiello G, Mandin P, Kim M, Scopelliti M, Inguanta R (2023) Behavior of a forest of NiFe nanowires in KOH and NaCl solution

for water electrolysis. Electrochim Acta 467:143120. https://doi.org/10.1016/j.electacta.2023.143120
6. Suleman F, Dincer I, Agelin-Chaab M (2015) Environmental impact assessment and comparison of some hydrogen production options. Int J Hydrogen Energy 40:6976–6987. https://doi.org/10.1016/j.ijhydene.2015.03.123
7. Bodo Z, Palotas BA (2016) Impact of the voltage fluctuation of the power supply on the efficiency of alkaline water electrolysis. ScienceDirect 41:11849–11856. https://doi.org/10.1016/j.ijhydene.2016.05.141
8. Ganci F, Baguet T, Aiello G, Cusumano V, Mandin P, Sunseri C, Inguanta R (2019) Nanostructured Ni based anode and cathode for alkaline water electrolyzers. Energies 12:3669. https://doi.org/10.3390/en12193669
9. Ganci F, Patella B, Cannata E, Cusumano V, Aiello G, Sunseri C, Mandin P, Inguanta R (2020) Ni alloy nanowires as high efficiency electrode materials for alkaline electrolyzers. Int J Hydrogen Energy 46:35777–35789. https://doi.org/10.1016/j.ijhydene.2020.11.208
10. Ursúa A, Gandía LM, Sanchis P (2012) Hydrogen production from water electrolysis: current status and future trends. Proc IEEE 100:410–426. https://doi.org/10.1109/JPROC.2011.2156750
11. Vogt H (2017) The quantities affecting the bubble coverage of gas-evolving electrodes. Electrochim Acta 235:495–499. https://doi.org/10.1016/j.electacta.2017.03.116
12. Zeng K, Zhang D (2010) Recent progress in alkaline water electrolysis for hydrogen production and applications. Prog Energy Combust Sci. 36:307–326. https://doi.org/10.1016/j.pecs.2009.11.002
13. Chandran P, Bakshin S, Chatterjee D (2015) Study on the characteristics of hydrogen bubble formation and its transport during electrolysis of water. Chem Eng Sci 138:99–109. https://doi.org/10.1016/j.ces.2015.07.041
14. Souza FR, Padilha CJ, Gonçalves SR, Souza OM, Rault-Berthelot J (2007) Electrochemical hydrogen production from water electrolysis using ionic liquid as electrolytes: towards the best device. J Power Sources 164:792–798. https://doi.org/10.1016/j.jpowsour.2006.11.049
15. Chang LN, Chung CP, Chuang JW, Hsu NCS, Sun WI, Chen YP (2016) Voltammetric study and electrodeposition of Ni(II)/Fe(II) in the ionic liquid 1-butyl-1-methylpyrrolidinium dicyanamide. J Electrochem Soc 163:9–16. https://doi.org/10.1149/2.0221602jes
16. Kumar SS, Himabindu V (2019) Hydrogen production by PEM water electrolysis – a review. Mater Sci Energy Technol 2:442–454. https://doi.org/10.1016/j.mset.2019.03.002
17. Maizi R, Fricoteaux P, Mohamadou A, Meddour A, Rousse C (2016) Electrode position of Ni, Fe and Ni-Fe alloys in two ionic liquids: (tri (n-butyl) [2-methoxy-2-oxoethyl] Ammonium bis (trifluoromethylsulfonyl) [BuGBOEt] [Tf2N] and (1-butyl-1-methylpyrrolidinium bis trifluoromethylsulfonyl) imide ([P1,4] [Tf2N]). Int J Electrochem Sci 11:7111–7124
18. Ray A, Saruhan B (2021) Application of ionic liquids for batteries and supercapacitors. Materials 14:2942. https://doi.org/10.3390/ma14112942
19. Miller AM, Wainright SJ, Savinell FR (2016) Communication—iron ionic liquid electrolytes for redox flow battery applications. J Electrochem Soc 163:578. https://doi.org/10.1149/2.0061605jes
20. Trombetta F, Souza OM, Souza FR, Martini AM (2019) Electrochemical behavior of aluminum in 1-n-butyl-3- methylimidazolium tetrafluoroborate ionic liquid electrolytes for capacitor applications. J Appl Electrochem 39:2315–2321. https://doi.org/10.1007/s10800-009-9954-7
21. Mohammad S, Hashemi H, Karnakok P, Hadikhani P, Chinello E, Litvinov S, Moser C, Koumoutsakos P, Psaltis D (2019) A versatile and membrane-less electrochemical reactor for the electrolysis of water and brine. Energy Environ Sci 12:1592–1604. https://doi.org/10.1039/C9EE00219G
22. Liu B, Liu X, Fan X, Ding J, Hu W, Zhong C (2020) 120 Years of nickel-based cathodes for alkaline batteries. J Alloy Compd 834:155185. https://doi.org/10.1016/j.jallcom.2020.155185
23. Zhang X, Zhu J, Wang Y, Wang J (2018) An experimental investigation of convective mass transfer characterization in two configurations of electrolyzers. ScienceDirect 43:8632–8643. https://doi.org/10.1016/j.ijhydene.2018.03.172
24. Siracusano S, Baglio V, Briguglio G, Brunaccini A, Diblasi A, Ornelas A, Trifoni E, Antonucci V, Arico AS (2012) An electrochemical study of a PEM stack for water electrolysis. Int J Hydrog Energy 27:1939–1946. https://doi.org/10.1016/j.ijhydene.2011.06.019
25. Hreiz R, Abdelouahed L, Funfschilling D, Lapicque F (2015) Electrogenerated bubble sinduced convection innarrow vertical cells: PIV measurementsand Euler-Lagrange CFD simulation. Chem Eng Sci 134:138–152. https://doi.org/10.1016/j.ces.2015.04.041
26. Wang H, Liu S, Huang K, Yin X, Peng S (2012) $BMIMBF_4$ ionic liquid mixtures electrolyte for Li-ion batteries. Int J Electrochem Sci 7:1688–1698. https://doi.org/10.1016/S1452-3981(23)13445-6
27. Mckerracher RD, Rodriguez HAF, Dimogiannis K, Alegre C, Villanueva-Martinez NI, Lázaro MJ, Baglio V, Aricó AS, Ponce LC (2021) Effect of 1-octanethiol as an electrolyte additive on the performance of the iron-air battery electrodes. J Solid State Electrochem 25:225–230. https://doi.org/10.1007/s10008-020-04738-4
28. Borba KN, Trombetta F, Souza RF, Martini EMA (2017) Stability of Al2O3/Al in ionic liquid $BMI.BF_4$/γ-butyrolactone electrolytes for use in electrolytic capacitors. Ionics 23:1165–1171. https://doi.org/10.1007/s11581-016-1912-x
29. Dupont J, Eberlin NM, Consortis SC, Santos SL (2006) The role of ionic liquids in co-catalysis of Baylis-Hillman reaction: interception of supramolecular species via electrospray ionization mass spectrometry. J Phys Org Chem 19:731–736. https://doi.org/10.1002/poc.1066
30. Loget G, Padilha CJ, Martini AE, Souza OM, Souza FR (2009) Efficiency and stability of transition metal electrocatalysts for the hydrogen evolution reaction using ionic liquids as electrolytes. Int J Hydrog Energy 34:84–90. https://doi.org/10.1016/j.ijhydene.2008.10.032
31. Souza FR, Loget G, Padilha CJ, Martini AE, Souza OM (2009) Molybdenum electrodes for hydrogen production by water electrolysis using ionic liquid electrolytes. Electrochem Commun 10:1673–1675. https://doi.org/10.1016/j.elecom.2008.08.029
32. Souza FR, Padilha CJ, Gonçalves SR, Dupont J (2003) Room temperature dialkylimidazolium ionic liquid-based fuel cells. Electrochem Commun 5:728–731. https://doi.org/10.1016/S1388-2481(03)00173-5
33. Abdelouahed L, Hreiz R, Poncin S, Valentin G, Lapicque F (2014) Hydrodynamics of gas bubbles in the gap of lantern blade electrodes without forced flow of electrolyte: experiments and CFD modelling. Chem Eng Sci 111:255–265. https://doi.org/10.1016/j.ces.2014.01.028
34. Chen Q, Lin W, Wang Z, Yu J, Li J, Wang Z (2022) Flow field characterization between vertical plate electrodes in a bench-scale cell of electrochemical water softening. Water Sci Technol 85:1736–1753. https://doi.org/10.2166/wst.2022.070
35. Berger A, Souza FR, Delgado RM, Dupont J (2001) Ionic liquid-phase asymmetric catalytic hydrogenation: hydrogen concentration effects on enantioselectivity. Tetrahedron: Asymm 12:1825–1828. https://doi.org/10.1016/S0957-4166(01)00341-X
36. Zhu M, Zhu M, Song Y, Liang W, Han W, Chen Y (2014) Viscosity of dimethylbenzene in [Bmim][$BF_4$] and [Bmim][PF6] ionic liquids. Appl Mech Mater 541:78–82. https://doi.org/10.4028/www.scientific.net/AMM.541-542.78

37. Sun D, Roth S, Black MJ (2014) A quantitative analysis of current practices in optical flow estimation and the principles behind them Int. J Comput Vis 106:115–137. https://doi.org/10.1007/s11263-013-0644-x
38. Zhang C, Chen Z, Wang M, Li M, Jiang S (2017) Robust non-local optical flow estimation with occlusion detection. IEEE Trans Image Process 26:4055–4067. https://doi.org/10.1109/ACCESS.2020.3045764
39. Li R, Tan R, Cheong L (2017) Robust optical flow estimation in rainy scenes. Proc Eur Conf Comput Vis 17:288–304. https://doi.org/10.48550/arXiv.1704.05239
40. Mei L, Lai J, Xie X, Zhu J, Chen J (2019) Illumination-invariance optical flow estimation using weighted regularization transform. IEEE Trans Circuits Syst Video Technol 30:495–508. https://doi.org/10.1109/tcsvt.2019.2890861
41. Zhen C, Ge L, Chen Z, Li M, Liu W, Chen H (2020) Refined TV-L optical flow estimation using joint filtering. IEEE Trans Multimedia 22:349–364. https://doi.org/10.1109/TMM.2019.2929934
42. Liu T, Shen L (2008) Fluid flow and optical flow. J Fluid Mech 614:253–291. https://doi.org/10.1017/S0022112008003273
43. Horn BK, Schunck BG (1981) Determining optical flow. Artif Intell 17:185–204. https://doi.org/10.1016/0004-3702(81)90024-2
44. Liu T (2017) An open source program for extraction of velocity fields from flow visualization images. J Open Res Softw 5:29. https://doi.org/10.5334/jors.168
45. Cheng C, Liu F, Zhong D, Hao G, Liu G, Li J (2022) Three-dimensional self-supporting catalyst with NiFe alloy/oxyhydroxide supported on high-surface cobalt hydroxide nanosheet array for overall water splitting. J Colloid Interface Sci 606:873–883. https://doi.org/10.1016/j.jcis.2021.08.020
46. Tang J, Jiang X, Tang L, Li Y, Zheng Q, Huo Y (2021) Self-supported wire-in-plate NiFeS/CoS nanohybrids with a hierarchical structure for efficient overall water splitting. Dalton Trans 50:5921–5930. https://doi.org/10.1039/d1dt00319d